Energy & Environmental Science

Accepted Manuscript

ROYAL SOCIETY OF CHEMISTRY

www.rsc.org/ees

Journal Name

RSCPublishing

ARTICLE

Light Trapping in Bendable Organic Solar Cells Using Silica Nanoparticle Arrays

Cite this: DOI: 10.1039/x0xx00000x

Jungheum Yun,*[a] Wei Wang,[b] Soo Min Kim,[c] Tae-Sung Bae,[d] Sunghun Lee,[a] Donghwan Kim,[c] Gun-Hwan Lee,[a] Hae-Seok Lee,*[c] and Myungkwan Song*[a]

Received 00th January 2012,
Accepted 00th January 2012

DOI: 10.1039/x0xx00000x

www.rsc.org/

A highly efficient light-scattering layer, composed of quasi-periodic discrete silica nanoparticles directly deposited onto polymer substrates to produce bendable organic solar cells (OSCs) with enhanced light absorption, is reported. A silica nanoparticle layer (SNL) underwent self-assembly on a highly flexible and heat-sensitive polymer at room temperature during fabrication, which employed a unique plasma-enhanced chemical vapour deposition technique. Such efficient light-scattering SNLs have not been realizable by conventional solution-based coating techniques. SNLs were optimized by precisely controlling dimensional parameters, specifically, nanoparticle layer thickness and interparticle distance. The optimized SNL exhibited an improved transmission haze of 16.8% in the spectral range of 350–700 nm, where reduction of the total transmission was suppressed to 2%. Coating light-scattering SNLs onto polymer substrates is a promising method for improving the light harvesting abilities of OSCs by enhancing the light absorption of photoactive polymer layers. This SNL-based flexible OSC exhibited a record power conversion efficiency (PCE) of 7.4%, representing a 13% improvement, while reducing the thickness of the photoactive polymer layer by 30%.

Broader context

Organic solar cells with thin photoactive polymer layers have attracted significant interest as inexpensive photovoltaic devices. Recent advances in technologies that utilize flexible polymer substrates for organic solar cells have enhanced the merits of low-cost, continuous roll-to-roll processes. However, flexible organic solar cells are still inefficient compared to their conventional inorganic counterparts. This is mainly because of their low power conversion efficiencies and long-term stabilities. The main reason for their low power conversion efficiencies is the low light harvesting efficiencies of semiconducting photoactive polymers used in organic solar cells. One solution is to enhance the photon absorption efficiencies of very thin photoactive polymer layers. Here, we propose a unique technique for fabricating silica nanoparticle-based light-scattering layers for use in highly efficient organic solar cells built on flexible polymer substrates. The direct and simple process used to deposit the silica nanoparticle arrays at room temperature is a cost-effective and high-throughput method for fabricating highly efficient light-scattering materials for use in flexible organic solar cells based on polymer substrates.

Introduction

Organic solar cells (OSCs) have received considerable attention because of their low weights, facile processing methods, strong low-light performances, and cost effectivenesses.[1] Combining OSCs with mechanically flexible polymer substrates further increases their technical appeal by facilitating high-throughput fabrication using large-area roll-to-roll processes.[2–4] OSCs exhibit relatively short energy payback times (0.79–2.02 years),[5–7] which represent the times required for modules to generate amounts of energy equivalent to those consumed during their manufacturing

phases.[8] Since they still have much lower power conversion efficiencies (PCEs) than any of their inorganic competitors, the energy payback time of OSCs can be further reduced by improving their PCEs. The PCEs of OSCs can be increased by incorporating low-bandgap photoactive polymers into them to extend their absorptions to longer wavelengths, namely to the edge of the visible range, up to 750 nm.[9–11] The PCEs of OSCs are significantly limited by the large discrepancies that exist between the light harvesting and charge collection efficiencies of photoactive polymers.[1,12–22] Nevertheless, photon absorptions can be improved by increasing the thickness of photoactive polymer layers; however, polymers with low charge carrier mobilities[23,24] and short exciton diffusion lengths[24] require layers to be as thin as possible to improve charge extraction efficiencies and suppress charge recombination.

The low PCEs of thin photoactive polymer layers with poor photon absorption efficiencies can be improved by enhancing their light-trapping properties. Increasing optical path lengths by extending oblique-angle scattering across photoactive polymers represents an effective light-trapping method.[1,17,22,25,26] When the dimensions of optically transparent nanostructures are comparable to the wavelengths of incident light, strong light scattering occurs as a result of morphology-dependent interference. This is known as Mie scattering.[1,25,27,28] Nanoscopic oxide nanoparticle arrays are considered excellent candidates for such applications because although they generate intensive forward scattering, they absorb and reflect very little of the incident light. Towards this end, the emergence of flexible OSCs has prompted the simple and inexpensive fabrication of light-scattering oxide nanoparticle arrays (ONAs) on polymer substrates.

However, light-scattering ONAs fabricated by conventional solution-based coating methods, which are usually considered to be cost-effective and scalable, are primarily being used on small glass substrates but not mechanically flexible, heat-sensitive polymer substrates.[25] Solution-based coatings of ONAs that exhibit efficient light-scattering capabilities, high light scattering, high transparency, and negligible reflection, have not yet been reported for use in flexible OSCs. The solution-based coating of ONAs onto polymer substrates calls for the precise control of various operating parameters, including the wettabilities of nanoparticle inks, evaporation rates of solvents, and distributions of nanoparticle stacks on polymer substrates. Optimal processing conditions differ greatly depending on the surface properties of the polymer substrate and working conditions. Any deviation from the optimal processing conditions results in irregularly distributed ONAs, which lack the desirable light-scattering properties. Such problems can result in poor reproducibility between batches, inconsistent ONA distributions on large-area polymer substrates, and poor light-scattering properties. Furthermore, because ONAs prepared by conventional solution methods are physically attached to chemically deactivated polymer surfaces, poor structural durability, which hinders the stable light scattering capabilities in flexible OSCs, is another concern. Although a unique solution-based wire-wound rod coating method[25] was recently reported to have solved these problems, the study did not provide experimental evidence that the flexible OSCs with light-scattering ONAs had improved PCEs. To conclude, solution-based coating methods used to obtain efficient light-scattering ONA layers on mechanically flexible, large-scale polymer substrates still possess significant challenges.

Therefore, a cost-effective and scalable alternative coating technology is required to produce highly efficient light-scattering ONAs on highly flexible, large-area polymer substrates. From the perspective of life-cycle energy consumption, which reflects the overall energy demand of producing solar cell modules, this alternative technology must be a simple, fast, and low-energy coating process. The successful candidate must be a high throughput, roll-to-roll compatible coating technique that utilizes the mechanical flexibilities of polymer substrates.

In this study, we report on a highly efficient light-scattering layer, composed of silica nanoparticles, that offers enhanced light absorption and, thus, photocurrent generation in flexible OSCs. Importantly, light-scattering silica nanoparticles with precisely controlled dimensions were found to simultaneously form and self-assemble on highly flexible and heat-sensitive poly(ethylene terephthalate) (PET) surfaces. Production was achieved using a room-temperature vacuum coating process that utilizes conventional plasma-enhanced chemical vapour deposition (PECVD). PECVD, which is highly compatible with continuous roll-to-roll processing, is already a mature fabrication technique that is used for coating inorganic layers onto large-area polymer substrates. This unique method, which utilizes PECVD, can resolve the abovementioned technical challenges that arise from the currently available solution-based coating techniques and facilitate cost-effective and high-throughput fabrication of light-scattering ONA coatings on large-area polymer substrates. Remarkably, a flexible OSC with light-scattering silica nanoparticles, fabricated using the room-temperature PECVD process proposed in this study, exhibited a PCE of 7.4%. The OSC had a 65 nm-thick photoactive polymer layer and demonstrated a PCE improvement of 13% and a photoactive polymer layer thickness reduction of more than 30%.

Experimental

Preparation of silica nanoparticle arrays

The light-scattering layer of the silica nanoparticle array was fabricated on 75 μm-thick PET (Panac, Co.) substrates composed of light incident surfaces. First, the PET surface was subjected to an Ar plasma-induced polymer pretreatment in a home-built PECVD system using a capacitively coupled radio frequency of 13.56 MHz.[29,30] The initiation was carried out with different durations of Ar plasma ignition, with a radio frequency power of 200 W (1.1 W cm^{-2}) and a working

pressure of 22.7 Pa. Next, the SNL was deposited on the plasma-treated PET surfaces.[29] The plasma power and pressure were kept constant during the subsequent silica coating process. Silica nanoparticles were grown with an O:Si atomic ratio of 1.9–2.0 at a deposition rate of 30 nm min^{-1} via the plasma polymerization of hexamethyldisiloxane (HMDSO, Sigma-Aldrich, 98% purity), which was thermally vaporized from a liquid HMDSO source in an evaporator (Bronkhorst High-Tech) at 130 °C, obtained from a gas mixture of HMDSO/O_2/Ar = 1.8:10:100 sccm. The surface temperature was no higher than 50 °C following the plasma pretreatment and silica deposition.

Fabrication of the organic solar cells

The OSCs consisted of a buffered layer of PEDOT-PSS (Clevios™ P) and a photoactive layer of PTB7 (1-Material Chemscitech):$PC_{71}BM$ (Solemme BV), fabricated on the underside of the PET substrates coated with Ag nanowires (NWs) as the transparent conducting electrode. Briefly, the Ag NW (Cambrios ClearOhm Ink) electrode (~66 nm thick) was prepared on the PET surface by spin coating at 800 rpm for 40 s. Then, 45 nm-thick PEDOT-PSS diluted in isopropyl alcohol (IPA) at a volume ratio of 1:2 was deposited on the Ag NW electrode by spin coating at 5000 rpm for 40 s. The active layer was spin coated at 1000 rpm using a mixture of PTB7:$PC_{71}BM$ (8 mg:12 mg), a heterojunction coating of an electron donor material: poly[[4,8-bis[(2-ethylhexyl)oxy]benzo[1,2-b:4,5-b'] dithiophene-2,6-diyl][3-fluoro-2-[(2-ethylhexyl)carbonyl] thieno[3,4-b]thiophenediyl]] (PTB7) and an electron acceptor material: [6,6]-phenyl-C_{71}-butyric acid methyl ester ($PC_{71}BM$), dissolved in 1 mL of chlorobenzene. The solution was further mixed with 1,8-diiodooctane in a 3% volume ratio prior to spin coating. The substrates were baked in a glove box at 100 °C for 5 min after each layer was spin coated. Finally, 0.7 nm-thick LiF and 100 nm-thick Al layers were deposited on the active layers by thermal evaporation in a vacuum of ~3 × 10^{-6} Torr. The device area, defined through a shadow mask of Al metal, was approximately 0.38 cm^2.

Characterization

The plane and cross-sectional morphologies of the polymer protrusions, SNLs, and Ag NWs were observed using field emission scanning electron microscopy (FE-SEM, Hitachi, S-5500) at the Korea Basic Science Institute (Jeonju, South Korea). The diameters of the silica nanoparticles were determined from the average values of three different surface domains (3 × 3 μm^2), analyzed by atomic force microscopy (AFM, Park System, XE-100) using the tapping mode at Changwon National University. The actual thicknesses of the SNLs were approximated from their cross-sectional FE-SEM images, and the nominal thicknesses of the silica planar layers, coated on Si wafers, were measured using a surface profiler (KLA-Tencor, P-11). The sheet resistance of the Ag NW electrode was measured at three different domains (2.0 × 2.0 cm^2) using a four-point probe system (Mitsubishi Chemical Co., MCP-T600) and was subsequently averaged. The specular and total transmission spectra of the SNLs and the Ag NWs, including the total reflection spectra of the SNLs, were measured in the wavelength range of 320–800 nm using ultraviolet-visible (UV) spectrophotometry (Varian, Cary 5000). The diffusive transmission was determined by subtracting the specular transmission from the total transmission. The transmission haze (H) was determined using the equation H (%) = T_D/T_T × 100, where T_D and T_T were the diffusive and total transmissions, respectively. The absorbance of the incident light in the photoactive layers was determined by ascertaining the total transmission and reflection. The mechanical bending test was performed to determine the variation in OSC performance. Using a custom-built two-point bending system, compressive stresses were induced by mechanical bending of the polymer substrates. The changes in the PCEs were measured as a function of the bending radii of the substrate. Three bending samples were examined and averaged for each OSC. The photovoltaic performances of the OSCs were determined using an air mass 1.5 global (AM 1.5 G) solar simulator (Oriel 300 W) with an irradiation of 100 mW cm^{-2}. This was adjusted with a reference monocrystalline Si solar cell (2 × 2 cm^2) calibrated at the National Renewable Energy Laboratory (NREL) (Colorado, USA). J–V curves were measured using a Keithley 2400 SourceMeter unit. The incident photon-to-current efficiency spectra were attained using a quantum efficiency measurement system (Oriel IQE-200), equipped with a 240 W quartz tungsten halogen lamp as the light source, a monochromator, an optical chopper, a lock-in amplifier, and a calibrated Si photodetector.

Optical simulation

The morphological effects of the SNL on the absorption of incident light in the photoactive layer were numerically predicted by ray-trace simulations using the Silvaco TCAD software package with a LUMINOUS 3D algorithm of the Atlas module. Complex optical properties including transmission, refraction, and absorbance of incident light along its propagation path were calculated using the refractive indices (n) and extinction coefficients (k) of the material layers through which the incident light penetrated.[31] The n and k values were determined experimentally for the PET and photoactive materials using spectroscopic ellipsometry (Ellipso Technology, Elli-SEU-am12) with the Lorentz oscillator dispersion model, while the n and k values of silica were adopted from the SOPRA database. The domain structure for optical simulation was designed so that the silica nanoparticles were superimposed on a thin silica layer continuously covering the surface of the PET substrate. The structural geometry of the silica nanoparticles was simplified as an elongated columnar structure with a semi-spherical top. The dimensions were approximated based on the data measured from cross-sectional FE-SEM images. The relative scale of diameter, height, and interparticle distance was 4:6:7 in 570 nm thick silica nanoparticles. The thickness of the continuous silica layer was fixed at 50 nm. The area of the

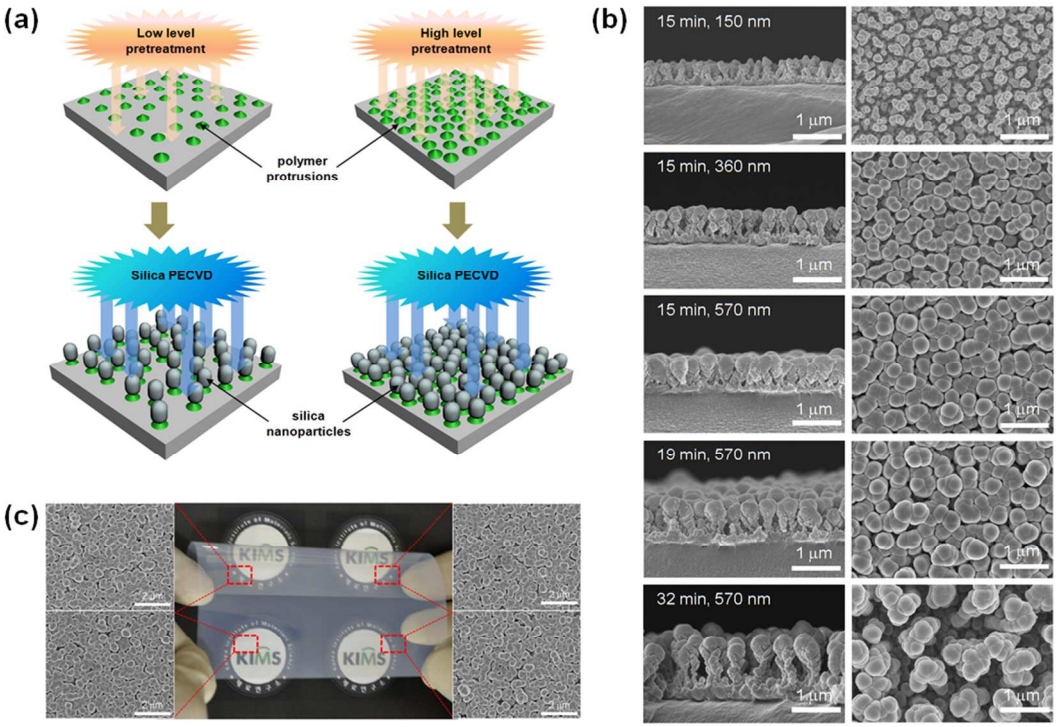

Fig. 1 (a) Schematic illustration of globular silica nanoparticles coated on PET substrates using a PECVD process. (b) Cross-sectional and plane FE-SEM images of SNLs at different nominal coating thicknesses, fabricated on PET surfaces that were plasma-treated for different time periods. Scale bar was 1 μm. (c) Optical image of a PET substrate overcoated with a light-scattering silica nanoparticle monolayer and plane-view FE-SEM images of the SNLs on four different spots. Scale bar was 2 μm.

calculation domain was 1 μm × 1 μm. Air mass 1.5 global was used as the incident light for the visible wavelength range between 350–800 nm.

Results and Discussion

The aim of the present study was to fabricate a highly efficient light-scattering SNL for bendable OSCs, using a simple vacuum deposition approach without the need for artificial nanopatterning or cumbersome solution-based techniques. The SNL fabrication on the PET substrate was accomplished by two sequential processes: (*i*) the formation of nanoscopic polymer protrusions by Ar plasma-induced pretreatment and (*ii*) the subsequent PECVD deposition of silica nanoparticles (**Fig. 1a**). A closely packed arrangement of nanoscopic polymer protrusions was formed on the top surface of the PET substrates, according to a well-known phenomenon associated with morphological modifications of surfaces during plasma treatment.[32–36] The formation of the protrusions was a result of the complex surface kinetics of low molecular-weight polymer chains, including chain scission and recombination, etching, migration, redeposition, and agglomeration under plasma-ion irradiation.[35–39] The ion energy and fluence applied in the polymer pretreatment were approximately 102 eV and 3.1 × 10^{17} cm^2 min^{-1}, respectively. We found that the dimensions and surface number density of the polymer protrusions changed progressively as the pretreatment time increased, owing to ion fluence. Furthermore, the protrusion evolution with increasing pretreatment time was accompanied by a reduction in the surface number density (**Fig. S1**). Here, jagged peak-like protrusions with dimensions of a few hundred nanometers evolved following plasma irradiation for 15–32 min. Hence, the mutual interdependence of the size and surface number density of the polymer protrusions was presumed to be a result of the continuous coalescence of neighboring protrusions with the highly volatile polymer surface. This effect has previously been associated with reduced interface free energy differences between the modified top surface and the underlying bulk.[29,40,41] Further details regarding the development of protrusions and their effects on chemical and morphological changes are described elsewhere.[35,36]

A unique morphological feature of the SNL growth was the self-assembly of a nearly quasi-periodic array of discrete silica nanoparticles on the plasma-treated PET surface (**Fig. 1a and 1b**). In this case, silica nanoparticles preferentially formed and evolved on the uppermost surface of the polymer protrusions with relatively large fluxes of gaseous organosilicon compounds arriving at the elevated polymer surface during the silica deposition. However, owing to the shadowed effects of the more rapidly growing silica nanoparticles on the neighboring polymer protrusions, severely reduced fluxes reached the recessed polymer between protrusions and thus suppressed the development of silica nanoparticles at the surface domains. We found that the silica

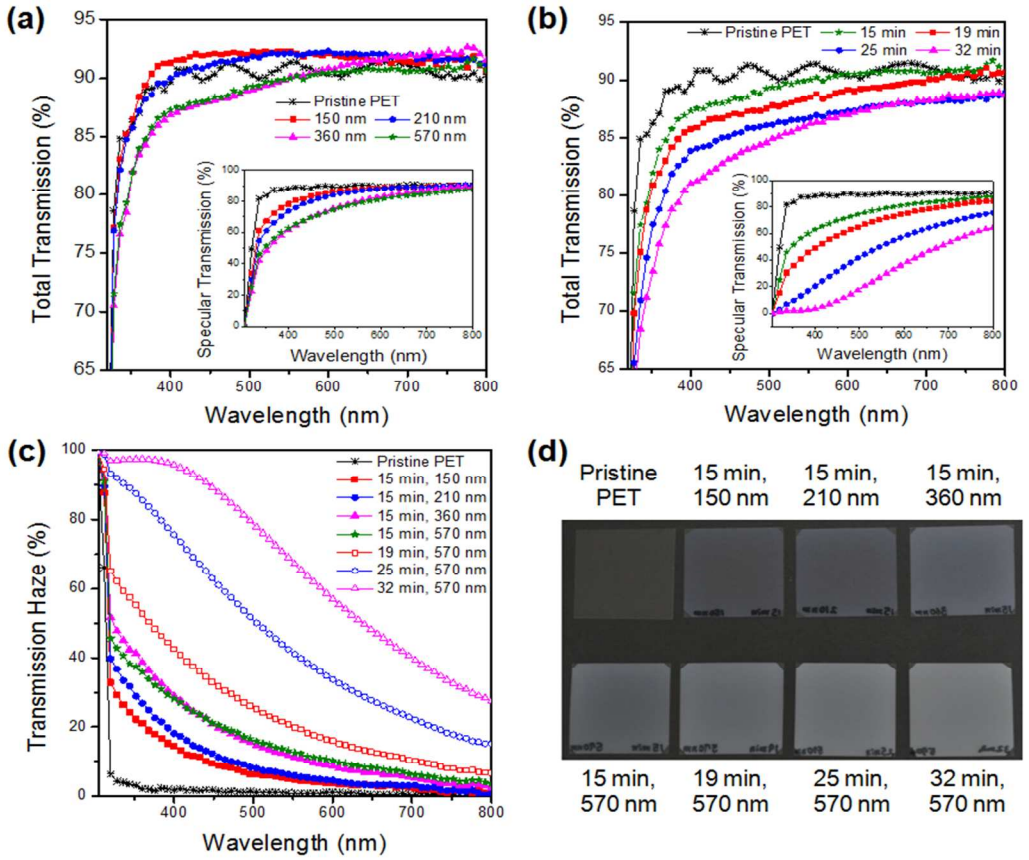

Fig. 2 Light-scattering characteristics of PET substrates overcoated by SNLs. Dependence of total transmission on (a) the nominal thickness of SNLs at a pretreatment time of 15 min and (b) the pretreatment time of the PET substrates coated with a 570-nm-thick SNL. (c) Transmission haze of the silica nanoparticle array for different layer thicknesses and pretreatment times. (d) Comparison of light-scattering between PET substrates overcoated with SNLs.

nanoparticles developed into larger nanoparticles on the protrusions and outgrew the remaining silica nanoparticles on the recessed surfaces. Another observed morphological feature was the globular-shaped geometry of the silica nanoparticles that displayed small contact areas at the topmost surface of the protrusions. Poor silica-PET adhesion, which is typically weaker than silica-silica cohesion, further restrained the lateral expansion of the growing silica nanoparticles along the surfaces. Furthermore, the geometry of the silica nanoparticles was driven towards a globular shape, reducing the overall surface energy of these nanoparticles. Notably, the selective growth mechanism of nanoparticles on polymer protrusions was observed for various oxide depositions using different vacuum deposition methods.[29,30,35,42]

This unique growth mechanism provides an opportunity to manipulate the morphological features of the silica nanoparticle array, which can directly alter its optical features. Thus, by controlling the pretreatment time of the PET substrates and the deposition thickness of the silica nanoparticles (**Fig. 1a and 1b**), we obtained silica nanoparticles with average diameters, which consistently increased with increased pretreatment times and deposition thicknesses (**Fig. S2**). However, such size evolution was accompanied by a clear reduction in the number density. The growth mechanism and the precise controllability of the SNL was successfully reproduced on a large-area flexible PET substrate with an area larger than 10 × 10 cm^2 (**Fig. 1c**). The surface of the PET substrate was fully covered by a uniform, close-packed SNL that exhibited highly efficient light-scattering in the visible spectral range. The uniformity of the SNL was verified by comparing its morphology across the PET substrate. Notably, this method is also compatible with high-throughput roll-to-roll coating processes that employ large-area flexible polymer substrates.

The light-scattering characteristics of PET substrates coated with SNLs were investigated at different PET substrate pretreatment times and with varying SNL thicknesses (**Fig. 2**). The specular and total transmission spectra were compared for SNL thicknesses between 150 nm and 570 nm at a constant pretreatment time of 15 min (**Fig. 2a**). The total transmission, combining specular and diffusive transmissions, decreased with increasing SNL thickness due to enhancements in the total reflection (**Fig. S3a**). The increase in SNL thickness caused more noticeable reductions in the specular transmission than in the total transmission. These differences

were a result of Mie scattering and corresponded to the increase in diffusive transmission (**Fig. S4a**).

The influence of pretreatment time on the transmissions was more significant than the change in SNL thickness. The total and specular transmissions decreased considerably with longer pretreatment times owing to increased reflection (**Fig. 2b and S3b**). Notably, an enhanced diffusive transmission was observed with longer pretreatment times. Specifically, the diffusive transmission reached 74% when the pretreatment time was increased to 32 min (at a wavelength of 450 nm) as a result of a significant difference between the total and specular transmissions (**Fig. S4b**). The degree of light scattering was further evaluated by comparing transmission hazes, diffusive to total transmissions, for varying pretreatment times and SNL thicknesses where a high transmission haze indicated high scattering (**Fig. 2c**). The increase in the transmission haze was nearly saturated when the SNL thickness was > 360 nm, whereas the transmission haze increased continuously for the entire range of the examined pretreatment times and reached 89.2% (at a wavelength of 450 nm; pretreatment time of 32 min). Although the transmission haze decreased with increasing wavelengths, the value still reached 48.3% at 650 nm. The enhancement of the light scattering in SNLs with increasing pretreatment time and SNL thickness was also clearly visualized upon comparison of the optical images (**Fig. 2d**). The high levels of light scattering could enable the production of high levels of photocurrent by enhancing the light trapping of the photoactive layers. However, the efficiency of the SNLs as light-scattering layers was constrained by a deleterious trade-off between the total transmission and the transmission haze, as an increase in the transmission haze was accompanied by a reduction in the total transmission.

The enhancement of the light scattering from the incident light in the SNL and its absorption in the photoactive layers was assessed experimentally and numerically. Here, 65 nm-thick PTB7:$PC_{71}BM$ was used as the photoactive layer. A clear improvement in the absorbance was observed in the photoactive layer with a 570 nm-thick SNL, coated on the light incident surface of the PET that had been plasma-treated for 15 min (**Fig. 3a**). To ascertain the contribution of the SNL to the light absorption, absorbance spectra were predicted theoretically for the photoactive layer in the presence and absence of the SNL (**Fig. 3b**). Computational simulations were carried out by applying the well-known ray-trace simulation method using the refractive indices and extinction coefficients of the SNL, PTB7:$PC_{71}BM$, and PET. The SNL geometry was simplified for the simulations by employing distinct silica nanoparticles with elongated columnar structures shown in the inset of Fig. 3b. The prediction of the change in the absorbance owing to the SNL was in good agreement with the experimental observation. The high absorbance in the photoactive layer was a result of the effective scattering enhancement in the SNL. The scattered lights crossed the photoactive layer at highly tilted angles. The large-angle propagation of the scattered lights elongated the path for the lights in the photoactive layer and thus enhanced their absorbance in the absorber when compared to the case without SNL (**Fig. 3c and 3d**). This indicated that the SNL positively contributed to the change in absorbance with enhanced light scattering, despite a non-negligible reduction in the optical transmission.

The improvement in the light absorption in the PTB7:$PC_{71}BM$ photoactive layer through nearly the entire visible spectra assured a high photocurrent generation from the OSCs using the photoactive layer. OSCs were fabricated on the underside of PET substrates with the architecture PET/Ag nanowires (Ag NWs)/poly(3,4-ethylenedioxythiophene):poly(styrenesulfonate) (PEDOT:PSS)/PTB7:$PC_{71}BM$/LiF/Al (**Fig. 4a**). The transparent conducting electrode, composed of Ag NWs with an average diameter of 25 nm and an average length of a few tens of micrometers, was spin-coated on the PET surface at a thickness of approximately 66 nm.[43] The AgNW electrode exhibited a sheet resistance and specular transmission of 12.7 Ω/sq^{-1} and 91.5% (at a wavelength of 550 nm), respectively. The light scattering owing to the Ag NW electrode was almost negligible as compared to that of the SNL, since its total transmission was measured as 93.5% at 550 nm.

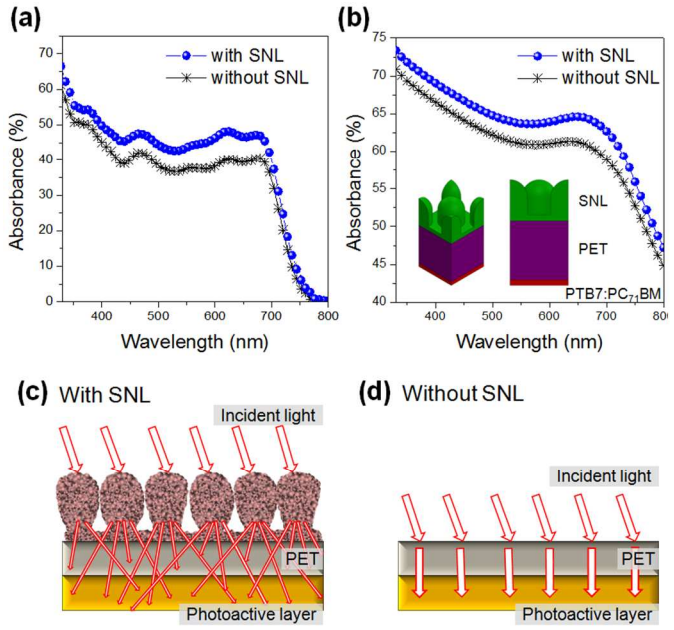

Fig. 3 (a) Experimental observation and (b) computational prediction for the improvement of optical absorption of incident light in a 65-nm-thick PTB7:$PC_{71}BM$ polymer layer, using 570 nm thick silica nanoparticles on the opposing side of PET substrates with a pretreatment time of 15 min. (inset) Schematic illustration of the computational simulations carried out by applying a simplified geometry, which consisted of elongated, hemispherical columns for the silica nanoparticle array. Schematics illustrate mechanisms for light propagation and absorption in the photoactive layer (c) with and (d) without SNL.

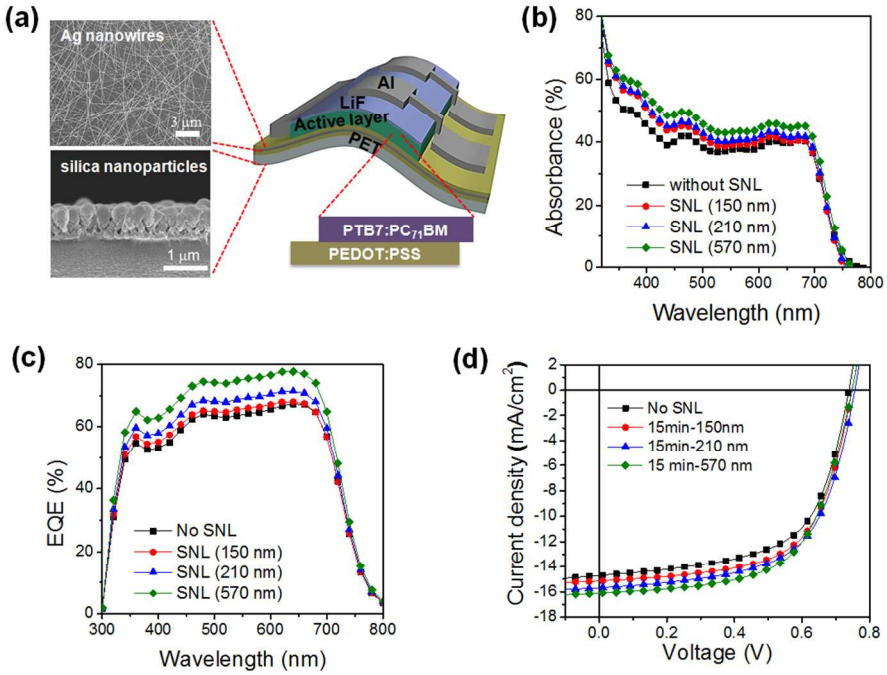

Fig. 4 (a) Device architecture of flexible OSC fabricated on a PET substrate using SNL as the light-scattering layer and a layer of Ag nanowires as the front electrode. Dependences of the (b) light absorbances of 95 nm-thick PTB7:PC71BM photoactive layers, along with PEDOT-PSS and LiF layers, and (c) EQE spectra and (d) *J-V* curves of the OSCs using the photoactive layers on different SNL thicknesses with a constant PET pretreatment time of 15 min.

The light absorbances, external quantum efficiency (EQE) spectra, and current density–voltage (*J–V*) characteristics of the OSCs using SNLs fabricated with different thicknesses were compared to estimate the effects of the SNL on the performances of the OSCs (**Fig. 4b–d**). Furthermore, the short-circuit current density (J_{sc}), open-circuit voltage (V_{oc}), fill factor (*FF*), and corresponding PCE were determined from the *J–V* characteristics (**Table 1**). The OSC using the SNL, optimized at a pretreatment time of 15 min with a silica thickness of 570 nm, exhibited the highest PCE of 7.42% at a PTB7:PC_{71}BM thickness of about 95 nm, whereas the OSC without SNL exhibited a PCE of 6.54%. The 13.5% increase was predominantly due to a J_{sc} increase from 14.76 to 16.15 mA cm^{-1}, which was a result of the absorbance enhancement owing to light scattering in the SNL. When the absorbance of incident light, scattered by SNLs with different thicknesses, was determined for the photo-absorbable multilayer of PEDOT:PSS/PTB7:PC_{71}BM/LiF, an increase in the SNL thickness contributed directly to the enhancement in the light absorbance in the multilayer, which led to a significant improvement in the EQE spectrum (**Fig. 4b and 4c**). The positive influence of the SNL on the light absorbance, and thus the EQE spectrum, could further improve in real OSC devices with an Al electrode owing to an optical resonant cavity occurring as a result of multiple round trips of incident light between the SNL and Al electrode. The EQE spectrum of

Table 1. Photovoltaic performance parameters of OSCs using SNLs fabricated with different silica thicknesses and PET pretreatment times, averaged for 5 specimens.

Pretreatment time [min]	SNL thickness [nm]	PTB7:PC_{71}BM thickness [nm]	J_{sc} [mA cm^{-2}]	V_{oc} [V]	FF [%]	R_{sh} [Ω cm^2]	R_s [Ω cm^2]	PCE [%]
0	0	95	14.76 ± 0.29	0.74 ± 0.02	60.23 ± 0.85	6.2×10^4	5.23	6.54 ± 0.06
15	150	95	14.99 ± 0.18	0.74 ± 0.01	62.39 ± 0.39	8.8×10^4	5.01	6.94 ± 0.13
15	210	95	15.68 ± 0.03	0.74 ± 0.01	61.81 ± 0.46	1.0×10^5	3.87	7.17 ± 0.08
15	360	95	15.97 ± 0.09	0.74 ± 0.01	61.32 ± 0.47	1.8×10^5	3.65	7.30 ± 0.09
15	570	95	16.15 ± 0.17	0.74 ± 0.02	61.55 ± 0.23	2.7×10^5	3.11	7.42 ± 0.05
19	570	95	16.07 ± 0.29	0.74 ± 0.01	60.96 ± 0.15	1.8×10^5	3.81	7.32 ± 0.12
25	570	95	16.02 ± 0.05	0.74 ± 0.01	61.42 ± 0.41	1.1×10^5	3.91	7.25 ± 0.09
32	570	95	16.02 ± 0.17	0.74 ± 0.01	61.23 ± 0.83	9.6×10^4	4.11	7.23 ± 0.09

Table 2. Photovoltaic performance parameters of OSCs fabricated with different photoactive polymer thicknesses, averaged for 5 specimens.

Pretreatment time [min]	SNL thickness [nm]	PTB7:$PC_{71}BM$ thickness [nm]	J_{sc} [mA cm^{-2}]	V_{oc} [V]	FF [%]	R_{sh} [Ω cm^2]	R_s [Ω cm^2]	PCE [%]
0	0	65	14.25 ± 0.08	0.72 ± 0.01	58.53 ± 1.23	3.3×10^4	7.23	6.02 ± 0.13
0	0	80	14.56 ± 0.14	0.73 ± 0.01	59.19 ± 0.45	5.2×10^4	5.93	6.27 ± 0.04
0	0	95	14.76 ± 0.29	0.74 ± 0.02	60.23 ± 0.85	6.2×10^4	5.23	6.54 ± 0.06
0	0	120	14.51 ± 0.18	0.72 ± 0.01	59.74 ± 0.04	4.2×10^4	6.33	6.22 ± 0.08
15	570	65	16.14 ± 0.18	0.74 ± 0.01	61.54 ± 0.27	2.6×10^5	3.30	7.40 ± 0.06
15	570	80	16.01 ± 0.11	0.74 ± 0.01	62.32 ± 0.70	2.7×10^5	3.21	7.42 ± 0.04
15	570	95	16.15 ± 0.17	0.74 ± 0.01	61.55 ± 0.23	2.7×10^5	3.11	7.42 ± 0.05
15	570	120	15.96 ± 0.02	0.73 ± 0.01	61.20 ± 0.77	2.2×10^5	3.52	7.17 ± 0.12

the OSC utilizing the optimized SNL exhibited a good photoconversion efficiency in the range of 350–700 nm, with an increase of 4.24–6.18% in EQE values as compared to the OSC without SNL. Notably, no apparent change was observed in the PCE when the thickness of the photoactive layer was reduced from 95 to 65 nm for the OSC using the optimized SNL, whereas a significant reduction in PCE with a thinner photoactive layer was clearly detected for the OSC without SNL (**Table 2**). The corresponding J_{sc} and *FF* values were analogous between the two PTB7:$PC_{71}BM$ thicknesses, and was attributed to the saturation of the absorbance enhancement owing to light scattering in the SNL as the PTB7:$PC_{71}BM$ thickness reached 65 nm.

The excellent flexibilities of the SNL on PET substrates ensured the structural durability of the OSC, and thus the photoconversion efficiency of the OSC, as it exhibited stability following exposure to extreme mechanical bending (**Fig. 5a**). The structural failures of oxide films deposited on polymer substrates during polymer deformation are usually ascribed to microscopic cracking and subsequent catastrophic delamination caused by poor adhesion between the oxide films and polymers.[44,45] However, no such failure was observed for the SNL even after repeatedly exposing the SNL to strain loading induced by bending the polymer substrate. The SNL consistently exhibited optical characteristics that were nearly independent of the strain loading. The total and regular transmission losses after 500 bending cycles at a minimum bending radius, *R*, of 1.1 mm were less than 1% and 3.5%, respectively, in the visible wavelength range (**Fig. 5b**). The PCE changes in the OSC were measured as a function of bending radius when the SNL and Ag NW were exposed to high stress, induced by mechanical bending of the PET substrate. The PCE of the OSC using the SNL decreased from 7.42 to 7.18%, which was comparable to the PCE reduction from 6.54 to 6.39% for the OSC without any SNL, even after exposure to R = 1.1 mm (**Fig. 5c**).

Conclusion

Light trapping using light-scattering nanostructures has emerged as a promising method to improve the photon absorption efficiencies in thin photoactive layers of OSCs. Here, we demonstrated the developement of a vacuum coating method that provided a simple, cost-effective, and high-throughput approach towards the fabrication of light-scattering layers on large substrates. The method permits the assembly of silica nanoparticle arrays on highly flexible and

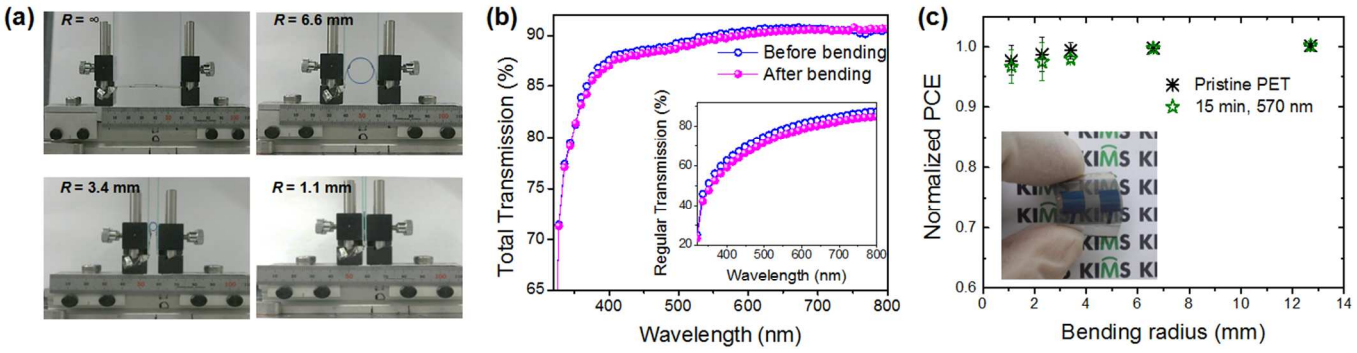

Fig. 5 (a) Photographs of an irreversible bending test of OSCs as a function of bending radius. (b) Changes in total and regular transmission spectra of 570 nm-thick SNLs, fabricated on PET substrates pretreated for 15 min, before and after 500 cyclic bending tests with a minimum bending radius of 1.1 mm. (c) Comparison of the PCEs as a function of bending radius during irreversible compressive bending (normalized to their initial values). The inset shows the flexible OSC used in this study.

heat-sensitive polymers, forming closely packed, nearly quasi-periodic silica nanoparticles through a unique self-assembly mechanism. By optimizing the nanoparticle size and interparticle distance with precisely controlled plasma pretreatment durations and silica deposition thicknesses, we obtained a silica nanoparticle array with an enhanced efficiency as the light-scattering layer. By employing the optimized pretreatment time of 15 min and deposition thickness of 570 nm, the resulting OSC exhibited a PCE of 7.42%, a 13.5% increase from that of an OSC without the silica nanoparticle array. This was attributed to the absorbance enhancement owing to the light scattering of the array. Therefore, the silica nanoparticle deposition method provides a way to achieve highly efficient light trapping in flexible OSCs.

Acknowledgements

This research was funded by internal grants from the Korea Institute of Materials Science (KIMS).

Notes and references

[a]*Surface Technology Division, Korea Institute of Materials Science, Changwon, Gyeongnam, 641-831, Republic of Korea. E-mail:jungheum@kims.re.kr; smk1017@kims.re.kr*
[b]*Institute of Hybrid Materials, The Growing Base for State Key Laboratory, Qingdao University, Qingdao, 266071, China.*
[c]*Department of Materials Science and Engineering, Korea University, Seoul, 136-713, Republic of Korea. E-mail: lhseok@korea.ac.kr*
[d]*Jeonju Center, Korea Basic Science Institute, Jeonju, Jeonbuk, 561-180, Republic of Korea*

†Electronic Supplementary Information (ESI) available: Cross-sectional FE-SEM images of polymer substrate, Three-dimensional AFM images of SNL morphologies, Total reflection spectra of PET substrate coated with SNL, Dependence of diffuse transmission spectra of PET substrates coated with SNL. See DOI: 10.1039/b000000x/

1. J. Weickert, R. B. Dunbar, H. C. Hesse, W. Wiedemann and L. Schmidt-Mende, *Adv. Mater.*, 2011, **23**, 1810-1828.
2. Y. Zhou, C. Fuentes-Hernandez, J. Shim, J. Meyer, A. J. Giordano, H. Li, P. Winget, T. Papadopoulos, H. Cheun, J. Kim, M. Fenoll, A. Dindar, W. Haske, E. Najafabadi, T. M. Khan, H. Sojoudi, S. Barlow, S. Graham, J.-L. Brédas, S. R. Marder, A. Kahn and B. Kippelen, *Science*, 2012, **336**, 327-332.
3. M. Jørgensen, K. Norrman, S. A. Gevorgyan, T. Tromholt, B. Andreasen and F. C. Krebs, *Adv. Mater.*, 2012, **24**, 580-612.
4. H. Jin, C. Tao, M. Velusamy, M. Aljada, Y. Zhang, M. Hambsch, P. L. Burn and P. Meredith, *Adv. Mater.*, 2012, **24**, 2572-2577.
5. D. Yue, P. Khatav, F. You and S. B. Darling, *Energy Environ. Sci.*, 2012, **5**, 9163-9172.
6. A. L. Roes, E. A. Alsema, K. Blok and M. K. Patel, *Progr. Photovolt.: Res. Appl.*, 2009, **17**, 372-393.
7. N. Espinosa, R. García-Valverde, A. Urbina and F. C. Krebs, *Sol. Energy Mater. Sol. Cells*, 2011, **95**, 1293-1302.
8. S. B. Darling and F. You, *RSC Adv.*, 2013, **3**, 17633-17648.
9. Y. Liang, Z. Xu, J. Xia, S.-T. Tsai, Y. Wu, G. Li, C. Ray and L. Yu, *Adv. Mater.*, 2010, **22**, E135-E138.
10. S. C. Price, A. C. Stuart, L. Yang, H. Zhou and W. You, *J. Am. Chem. Soc.*, 2011, **133**, 4625-4631.
11. H. Zhou, L. Yang, A. C. Stuart, S. C. Price, S. Liu and W. You, *Angew. Chem.*, 2011, **123**, 3051-3054.
12. A. J. Moulé, J. B. Bonekamp and K. Meerholz, *J. Appl. Phys.*, 2006, **100**, 094503.
13. L. Müller-Meskamp, Y. H. Kim, T. Roch, S. Hofmann, R. Scholz, S. Eckardt, K. Leo and A. F. Lasagni, *Adv. Mater.*, 2012, **24**, 906-910.
14. G. Li, V. Shrotriya, Y. Yao and Y. Yang, *J. Appl. Phys.*, 2005, **98**, 043704.
15. K. M. Coakley and M. D. McGehee, *Chem. Mater.*, 2004, **16**, 4533-4542.
16. D.-H. Ko, J. R. Tumbleston, A. Gadisa, M. Aryal, Y. Liu, R. Lopez and E. T. Samulski, *J. Mater. Chem.*, 2011, **21**, 16293-16303.
17. K. S. Nalwa and S. Chaudhary, *Optics Express*, 2010, **18**, 5168-5178.
18. K.-S. Liao, S. D. Yambem, A. Halder, N. J. Alley and S. A. Curran, *Energies*, 2010, **3**, 1212-1250.
19. L. A. A. Pettersson, L. S. Roman and O. Inganäs, *J. Appl. Phys.*, 1999, **86**, 487-496.
20. T. Stübinger and W. Brütting, *J. Appl. Phys.*, 2001, **90**, 3632-3641.
21. A. P. Smith, R. R. Smith, B. E. Taylor and M. F. Durstock, *Chem. Mater.*, 2004, **16**, 4687-4692.
22. P.-C. Tseng, M.-H. Hsu, M.-A. Tsai, C.-W. Chu, H.-C. Kuo and P. Yu, *Org. Electron.*, 2011, **12**, 886-890.
23. R. J. Kline, M. D. McGehee, E. N. Kadnikova, J. Liu and J. M. J. Fréchet, *Adv. Mater.*, 2003, **15**, 1519-1522.
24. H. Hoppe and N. S. Sariciftci, *J. Mater. Res.*, 2004, **19**, 1924-1945.
25. S. Jeong, L. Hu, H. R. Lee, E. Garnett, J. W. Choi and Y. Cui, *Nano Lett.*, 2010, **10**, 2989-2994.
26. V. E. Ferry, M. A. Verschuuren, M. Claire van Lare, R. E. I. Schropp, H. A. Atwater and A. Polman, *Nano Lett.*, 2011, **11**, 4239-4245.
27. G. Mie, *Ann. Phys.*, 1908, **25**, 377-445.
28. S. M. Scholz, R. Vacassy, J. Dutta, H. Hofmann and M. Akinc, *J. Appl. Phys.*, 1998, **83**, 7860-7866.
29. J. Yun, T.-S. Bae, J.-D. Kwon, S. Lee and G.-H. Lee, *Nanoscale*, 2012, **4**, 7221-7230.
30. J. Yun, Y. H. Park, T.-S. Bae, S. Lee and G.-H. Lee, *ACS Appl. Mater. Interfaces*, 2013, **5**, 164-172.
31. K. S. Yee, *IEEE Trans. Antennas Propag*, 1966, 14, 302-307.
32. U. Schulz, P. Munzert, R. Leitel, I. Wendling, N. Kaiser and A. Tünnermann, *Opt. Express*, 2007, **15**, 13108-13113.
33. B. Gupta, J. Hilborn, C. H. Hollenstein, C. J. G. Plummer, R. Houriet and N. Xanthopoulos, *J. Appl. Polym. Sci.*, 2000, **78**, 1083-1091.
34. M. Collaud Coen, R. Lehmann, P. Groening and L. Schlapbach, *Appl. Surf. Sci.*, 2003, **207**, 276-286.
35. J. Yun, S. Lee, T.-S. Bae, Y. Yun, S. Lee, J.-D. Kwon and G.-H. Lee, *Plasma Process. Polym.*, 2011, **8**, 815-831.
36. J. Yun, T.-S. Bae, S. Lee, S. Lee, J. Rha and G.-H. Lee, *Plasma Process. Polym.*, 2012, **9**, 135-148.

37. C. H. Bichler, H.-C. Langowski, U. Moosheimer and B. Seifert, *J. Adhes. Sci. Technol*., 1997, **11**, 233-246.
38. S. Weidner, G. Küehn, R. Decker, D. Roessner and J. Friedrich, *J. Polym. Sci*., *Part A*: *Polym. Chem*., 1998, **36**, 1639-1648.
39. Q. T. Le, J. J. Pireaux, R. Caudano, P. Leclere and R. Lazzaroni, *J. Adhes. Sci. Technol*., 1998, **12**, 999-1023.
40. O. D. Greenwood, J. Hopkins and J. P. S. Badyal, *Macromolecules*, 1997, **30**, 1091-1098.
41. R. D. Boyd and J. P. S. Badyal, *Macromolecules*, 1997, **30**, 3658-3663.
42. W. Wang, T.-S. Bae, Y. H. Park, D. H. Kim, S. Lee, G. Min, G.-H. Lee, M. Song and J. Yun, *Nanoscale*, 2014, **6**, 6911-6924.
43. M. Song, D. S. You, K. Lim, S. Park, S. Jung, C. S. Kim, D.-H. Kim, D.-G. Kim, J.-K. Kim, J. Park, Y.-C. Kang, J. Heo, S.-H. Jin, J. H. Park and J. W. Kang, *Adv. Funct. Mater*., 2013, **23**, 4177-4184.
44. Y. Leterrier, *Prog. Mater. Sci*., 2003, **48**, 1-55.
45. J. Lewis, *Mater. Today*, 2006, **9**, 38-45.

Graphical Abstract

Light Trapping in Bendable Organic Solar Cells Using Silica Nanoparticle Arrays

Jungheum Yun, Wei Wang, Soo Min Kim, Tae-Sung Bae, Sunghun Lee, Donghwan Kim, Gun-Hwan Lee, Hae-Seok Lee, Myungkwan Song

A highly efficient light-scattering layer based on silica nanoparticle array was fabricated on a flexible polymer substrate by employing a direct vacuum deposition process at room temperature, facilitating a power conversion efficiency of 7.42% from a flexible organic solar cell.

ToC figure